

Perspective

# Plasmonic Field-Effect Transistors (TeraFETs) for 6G Communications

Michael Shur <sup>1,2,\*</sup>, Gregory Aizin <sup>3</sup>, Taiichi Otsuji <sup>4</sup> and Victor Ryzhii <sup>4,5</sup>

<sup>1</sup> Rensselaer Polytechnic Institute, Troy, NY 12180, USA

<sup>2</sup> Electronics of the Future, Inc., Vienna, VA 22181, USA

<sup>3</sup> Kingsborough College, The City University of New York, Brooklyn, NY 11235, USA;  
gregory.aizin@kbcc.cuny.edu

<sup>4</sup> Research Institute of Electrical Communication, Tohoku University, Sendai 980-8577, Japan;  
otsuji@riec.tohoku.ac.jp (T.O.); v-ryzhii@riec.tohoku.ac.jp (V.R.)

<sup>5</sup> Institute of Ultra High Frequency Semiconductor Electronics of RAS, 117105 Moscow, Russia

\* Correspondence: shurm@rpi.edu or michael.shur@electronicsoffuture.com

**Abstract:** Ever increasing demands of data traffic makes the transition to 6G communications in the 300 GHz band inevitable. Short-channel field-effect transistors (FETs) have demonstrated excellent potential for detection and generation of terahertz (THz) and sub-THz radiation. Such transistors (often referred to as TeraFETs) include short-channel silicon complementary metal oxide (CMOS). The ballistic and quasi-ballistic electron transport in the TeraFET channels determine the TeraFET response at the sub-THz and THz frequencies. TeraFET arrays could form plasmonic crystals with nanoscale unit cells smaller or comparable to the electron mean free path but with the overall dimensions comparable with the radiation wavelength. Such plasmonic crystals have a potential of supporting the transition to 6G communications. The oscillations of the electron density (plasma waves) in the FET channels determine the phase relations between the unit cells of a FET plasmonic crystal. Excited by the impinging radiation and rectified by the device nonlinearities, the plasma waves could detect both the radiation intensity and the phase enabling the line-of-sight terahertz (THz) detection, spectrometry, amplification, and generation for 6G communication.

**Keywords:** 6G communications; plasmonic crystals; field-effect transistor arrays; plasma wave instabilities; terahertz detection; terahertz generation; line-of-sight detection; silicon CMOS; travelling wave amplifier; terahertz radiation



**Citation:** Shur, M.; Aizin, G.; Otsuji, T.; Ryzhii, V. Plasmonic Field-Effect Transistors (TeraFETs) for 6G Communications. *Sensors* **2021**, *21*, 7907. <https://doi.org/10.3390/s21237907>

Academic Editors: Maris Bauer and Fabian Friederich

Received: 21 October 2021

Accepted: 16 November 2021

Published: 27 November 2021

**Publisher's Note:** MDPI stays neutral with regard to jurisdictional claims in published maps and institutional affiliations.



**Copyright:** © 2021 by the authors. Licensee MDPI, Basel, Switzerland. This article is an open access article distributed under the terms and conditions of the Creative Commons Attribution (CC BY) license (<https://creativecommons.org/licenses/by/4.0/>).

## 1. Introduction

Within literally one generation, the Internet revolutionized our lives and proved to be a lifesaver during the COVID-19 pandemic. The wireless communication during the pandemic increased about 40%. Teleconferencing increased by about 300% [1]. It was mostly enabled by one material—silicon—and by one device—the field-effect transistor—albeit with a lot of help from germanium, III–V, and some other materials. We now use 4G and emerging 5G technology, but the 6G communications will be another transformational jump in communications (see Figure 1). 6G will raise applications in telemedicine, teleconferencing, defense, industrial controls, cyber security, the Internet of Things, autonomous unmanned cars, robotics and stay-at-home work and conferencing to a much higher level [2–11]. 6G will expand the wireless high-speed communications to the space, sea, and upper atmosphere.

Analyzing the spectrum of possible pandemic outcomes using the Pandemic Equation [12] shows that the pandemic tail and even possible spikes might still be with us for years to come driven by new emerging COVID-19 virus variants, such as the Delta variant. This makes the planned transition to the 6G communications using the sub-terahertz (sub-THz) range to be even more important. This 300 GHz range has been identified as the range between 252.72 GHz to 321.84 GHz [13].

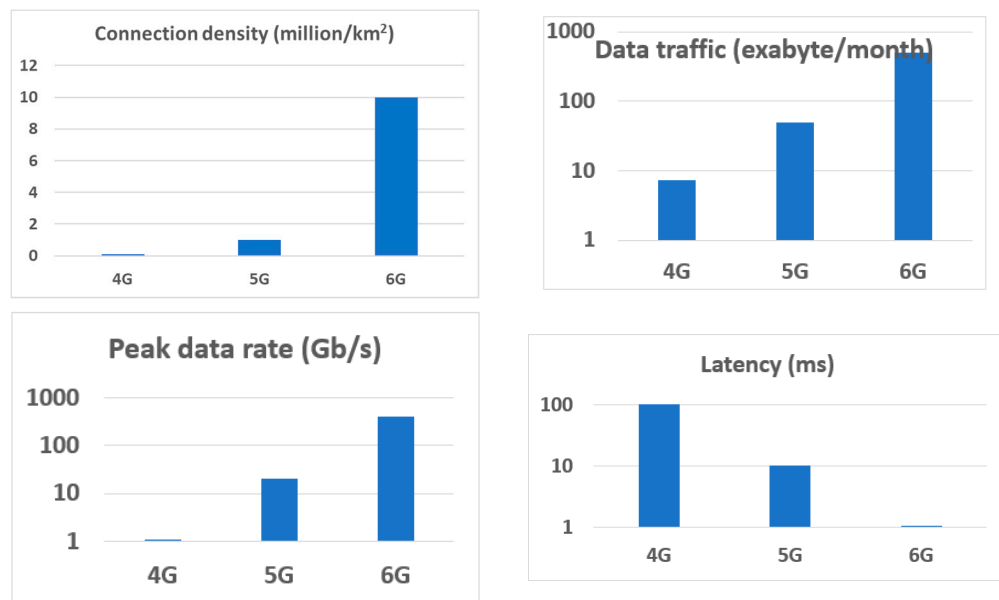


**Figure 1.** Communication evolution from 4G to 6G.

Among the technologies to support such a transition, the plasmonic crystal technology has the potential to become a winner. A unit cell of such a crystal has small dimensions to support the ballistic or quasi-ballistic transport and plasmonic resonances, while the overall size of the crystal is sufficiently large to efficiently capture or emit a sub-THz or a THz beam (see Figure 2) [14–33].

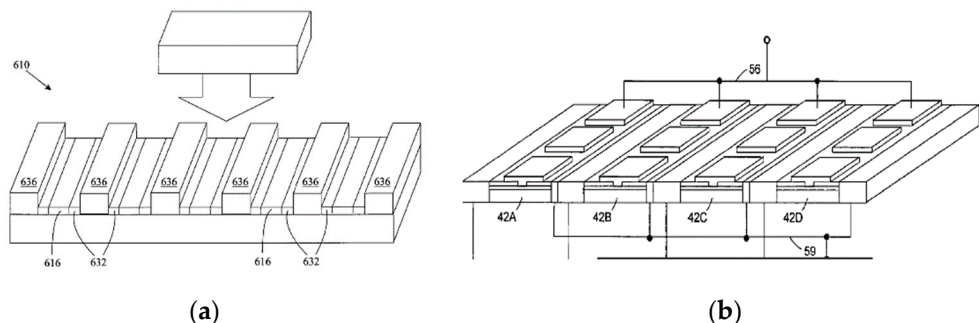


**Figure 2.** Plasmonic crystal concept: multi finger (grating gate) (from [14]) (a) and two-dimensional plasmonic array (from [15]) (b).

For example, the critical unit cell dimensions for silicon at room temperature might be on the order of 20 to 50 nm depending on the mobility and electron density. For the 240 to 320 GHz range, the overall dimension of the plasmonic crystal device could be in the millimeter range. Unique circuit applications for the plasmonic crystal devices could range from the line-of-sight detection [34], spectroscopy [35,36], homodyne [37–39] or heterodyne detection [40–43], frequency to digital conversion [44], and travelling wave amplifiers [45].

Plasma waves were first predicted by Tonks and Langmuir in 1929 [46]. In 1952, David Pines and David Bohm introduced the term “plasmon” [47]. The seminal works of Stern and Ferrell [48] and Chaplik [49] considered plasma waves in semiconductors. The promise and demonstrations of the THz generation by unstable resonant plasma waves [50–60], and of the THz detection by both resonant [61–66] and decaying [67–84] plasma waves has stimulated a lot of interest to this research area and resulted in the demonstration of the THz plasmonic detection in Si [70–75], III-V [76–78], III-N [79–82], monolayer, bilayer, and bipolar graphene [64,65,85–90]. In this paper, we analyze the applications of this technology for future 6G communications.

## 2. Plasmonic TeraFETs

Field-effect transistors operating in plasmonic regimes and often referred to as TeraFETs have already demonstrated an impressive performance in the sub-THz and THz range (see Table 1).

**Table 1.** TeraFET detector performance at sub-THz and THz frequencies (data from [82]).

Detector Type	Frequency (THz)	Noise Equivalent Power (pW/Hz <sup>1/2</sup> )
AlGaN/GaN TeraFETs	0.49–0.65	25–31
AlGaN/GaN TeraFETs	0.7–0.9	30–50
65 nm Si CMOS	0.8–1	100
65 nm Si CMOS	0.65	17
65 nm Si CMOS	0.72	14
90 nm Si CMOS	0.6	48–70
130 nm Si CMOS	0.26	8.4

Grated gate structures [14–33,77,78,89–91] demonstrated a better performance compared to single TeraFETs and a promise of THz radiation. Most of the room temperature results are for damped plasma wave detection by field-effect transistors. Figure 3 presents the largest calculated resonant quality factors for the single TeraFETs and the plasmonic frequencies at which these maximum quality factors are obtained.

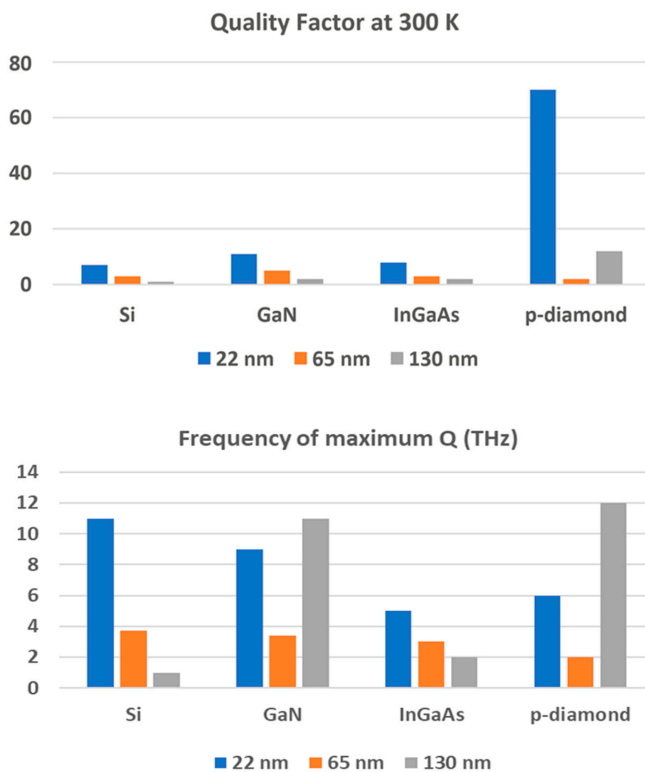


**Figure 3.** Estimated values of the maximum quality factor  $Q_m$ , and the frequency at which this value is achieved,  $f_m$ , for Si, GaN, InGaAs, and p-diamond TeraFETs (data from [92,93]). Parameters used in the calculation: mobilities for Si  $0.1450 \text{ m}^2/\text{Vs}$ , for GaN  $0.2 \text{ m}^2/\text{Vs}$ , for InGaAs  $1.2 \text{ m}^2/\text{Vs}$ , and for p-diamond  $0.53 \text{ m}^2/\text{Vs}$ ; effective masses: for Si 0.19, for GaN 0.23, for InGaAs 0.041, and for p-diamond 0.663.

The quality factor values,  $Q$ , shown in Figure 3, were obtained using the following equation:

$$Q = \omega_p \tau_{eff} \quad (1)$$

Here  $\omega_p = sk$  is the plasma velocity,  $k = \pi/(2L)$  is the wave vector of the fundamental plasmonic mode for a TeraFET detector, and  $s$  is the plasma wave velocity:

$$s = v_{th} ((1 + \exp[-qU_o/(\eta k_B T)]) \ln[1 + \exp[qU_o/(\eta k_B T)]])^{0.5} \quad (2)$$

$U_o = U_g - U_T$  is the gate voltage swing,  $U_g$  is the gate-to-source voltage,  $U_g - U_T$  is the threshold voltage,  $h$  is the subthreshold ideality factor,  $1/\tau_{eff} = 1/\tau_m + \nu k^2$  is the effective scattering frequency,  $\nu$  is the electron fluid viscosity,  $L$  is the channel length,  $\tau_m = \mu m/q$  is the momentum relaxation time,  $m$  is the low field mobility,  $m$  is the electron effective mass,  $q$  is the electronic charge,  $k_B$  is the Boltzmann constant, and  $T$  is the temperature.

The quality factors in Figure 3 are much smaller than that for the photonic crystals operating in near infrared or visible range and using, for example, gold nanoparticles [94]. Moreover, the values in Table 2 represent the upper bound of the quality factors of the THz TeraFETs that could be achieved. Parasitic elements [95], surface scattering [96], quantum reflection [97] from the contact regions all conspire to reduce the quality factors. Oblique waves were mentioned as another reason for the quality factor reduction [98], which, however, was not confirmed by numerical simulations [99]. For example, the calculation in [91,92] predicts the quality factor for InGaAs at 77 K of 18. In fact, the measured quality factor at 110 K was 1.4 [100]. The resonant behavior for Si TeraFETs at room temperature for the 20 nm NMOS ( $Q = 7$ ) is predicted for 11 THz, which is a larger frequency than the optical phonon frequency in Si (~8 THz). At such frequency, coupling with lattice vibrations should be accounted for. However, the data in Figure 3 provide the guidance for searching for the resonant plasmonic response at room temperature.

**Table 2.** Performance of THz detection devices (data from [101–103]).

THz Detector	Mechanism	Speed	Operating Temperature (K)	Responsivity (kV/W or A/W)	NEP (pW/Hz <sup>-1/2</sup> )
Golay cell	Thermal	Slow	300	10–100 kV/W	~100
Bolometer	Thermal	Slow	4.2	~100 kV/W	~0.1
Schottky diode	Rectification	Fast	300	0.1 to 1.5 kV/W	2.7 to 40
GaN TeraFET	Plasmonic	Fast	300	1.1 kV/W	40
Grated Gate TeraFET	Plasmonic	Fast	300	2.2 to 23 kV/W	0.5 to 50
Resonant tunnelling diode	Resonant tunnelling	Fast	300	7.3 A/W	7.7
Resonant tunnelling diode	Resonant tunnelling	Fast	300	0.9 kV/W	2.5

Table 2 compares the performance of THz TeraFET detectors with other THz detectors. As seen, the achieved TeraFET performance is at or above the state-of-the-art. Since the TeraFET technology is still developing, it is expected to become a leading THz detection technology. In addition to fast speed, tunability, and operating in a wide temperature range, possibly the greatest advantage of TeraFETs is the compatibility with the Si CMOS technology. All THz communication components, detectors, generators, and modulators operating in the 300 GHz band could be implemented using Si CMOS TeraFETs. This makes this technology especially appealing for the 6G communication integrated circuits.

The bandwidth is determined by the received power,  $P_r$ , the signal-to-noise ratio,  $SN$ , and the detector noise equivalent power,  $NEP$  [104].

$$BW = \frac{P_r^2}{SN^2 NEP^2} \quad (3)$$

$$P_r = \frac{c^2 G_r G_t P_t}{A(4\pi R f)^2} \quad (4)$$

Here,  $P_t$  is the transmitted power,  $c$  is the speed of light,  $G_r$  and  $G_t$  is the receiving and transmitting antenna gains,  $A$  is the propagation loss,  $R$  is the communication distance, and  $f$  is the communication frequency. The state-of-the-art Si FET emitters using frequency multiplication generate in the order of a hundred of microwatts power in the 300 GHz range [105,106]. However, the TeraFET output power could be increased using a series connection of TeraFETs [107] and even more by using the plasmonic crystal TeraFETs discussed in the next section with the estimated power output on the order  $\sim 100$  mW [20]. Calculations using Equations (3) and (4) show that this power might be sufficient if the receiver NEP could be reduced to  $0.1$  pW/Hz $^{1/2}$  from the current value of  $0.5$  pW/Hz $^{1/2}$  (see Table 1). As seen from Equations (3) and (4), this increase in the transmitted power enable orders of magnitude increases in the bandwidth and/or in the communication range.

TeraFETs could detect and generate THz radiation. However, their modulation speed is limited by the transistor cutoff frequency,  $f_T$  [108]. The upper bound of  $f_T$  is given by [108]:

$$f_{To} = \frac{v_s}{2\pi L} \quad (5)$$

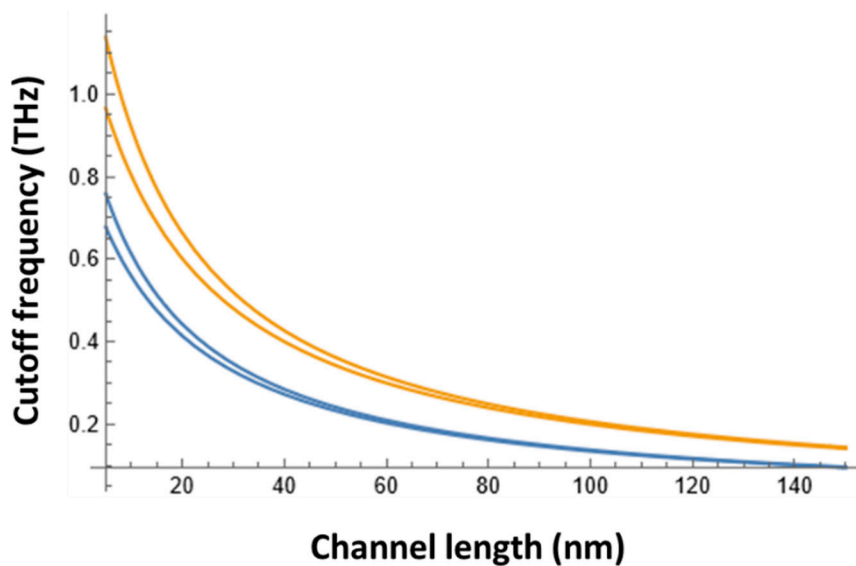
where  $L$  is the channel length and  $v_s$  is the electron saturation velocity. For silicon longer channel devices,  $v_s$  is  $\sim 10^5$  m/s and could be  $\sim 50\%$  higher in short-channel devices [109]. However, as shown in [110], the maximum modulation frequency peaks at the inverse effective electron relaxation time, which was taken as the electron momentum relaxation time,  $\tau_m = m\mu/q$ , where  $m$  is the electron effective mass.

The contribution of this effect into  $f_T$  could be estimated as follows:

$$f_T = \frac{1}{1/f_{To} + \tau_m} \quad (6)$$

Figure 4 shows dependence of the cutoff frequency on the channel length for  $v_s = 10^5$  m/s and  $v_s = 1.5 \times 10^5$  m/s with and without accounting for the electron momentum relaxation time. As seen, Si TeraFETs could be modulated at sub-THz frequency, enabling their application for the 300 GHz band 6G communication.

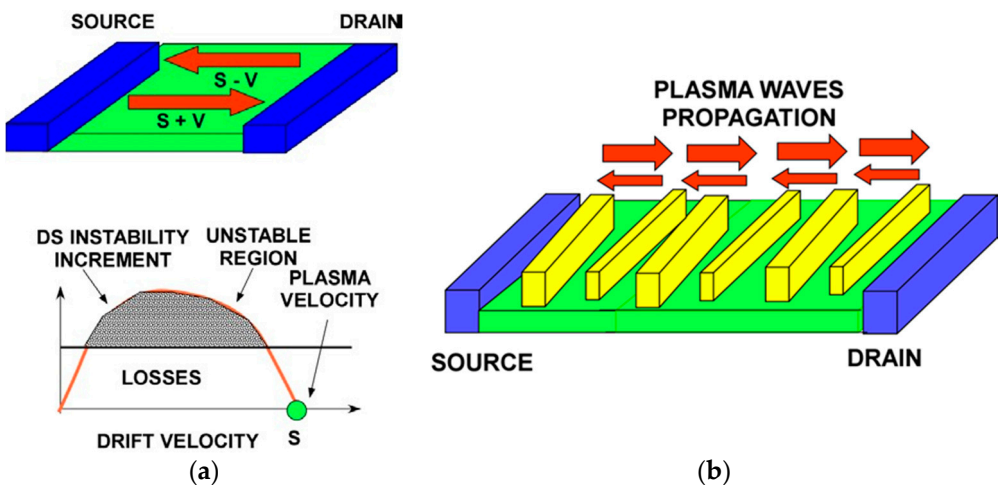
(The bandwidth is  $BW \approx 2f_T$ , since the TeraFETs could be modulated at frequencies on the order of  $f_T$ .)



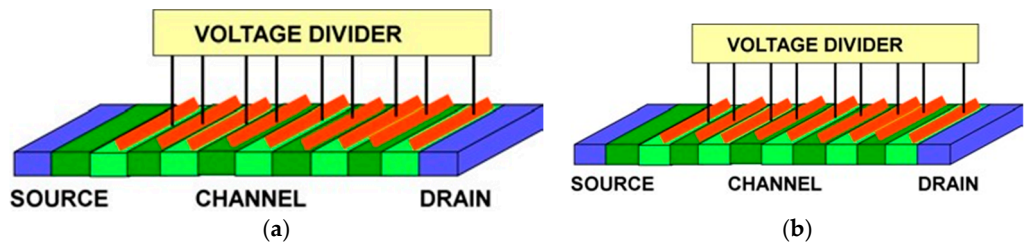
**Figure 4.** Dependence of the cutoff frequency on the channel length for  $v_s = 10^5$  m/s (two bottom curves) and  $v_s = 1.5 \times 10^5$  m/s (two top curves) with (bottom line in each set) and without (top line in each set) accounting for the electron momentum relaxation time.

### 3. Plasmonic Crystals

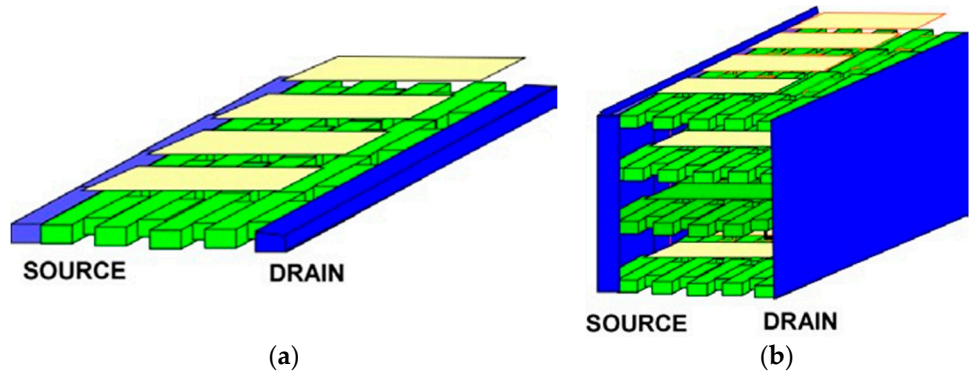
Figures 5–8 show different plasmonic crystal implementations proposed for detecting, processing, and generating the THz radiation. Figure 5 illustrated the Dyakonov–Shur (DS) instability mechanism [50] that relies on the difference in the reflection coefficients from the channel boundaries due to the differences in the velocities of the plasma waves propagating from the source to the drain ( $s + v$ ) and reflected from the drain ( $s - v$ ). Here,  $v$  is the electron drift velocity. The largest increment corresponds to the boundary conditions of the short-circuited source and open drain. Having finite impedances at the source and drain reduces the increment [111,112].



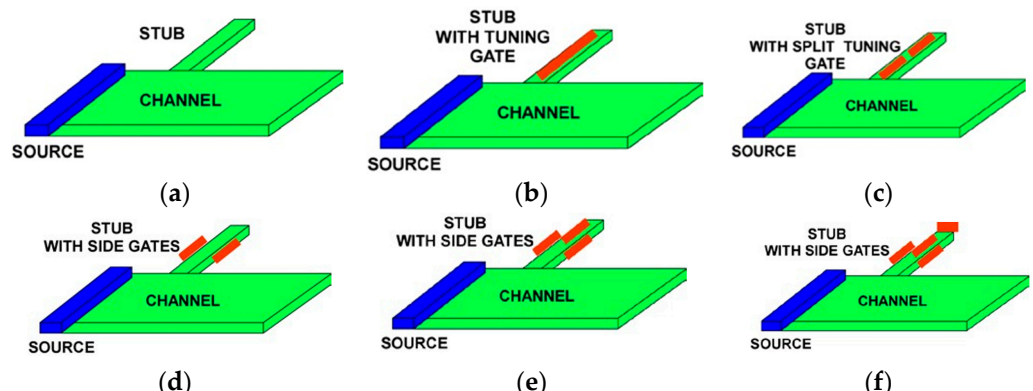
**Figure 5.** The Dyakonov–Shur (DS) instability increment (a) and 1D plasmonic crystal implementation (b).



**Figure 6.** Plasmonic boom: variable electron sheet density (a) and variable width structures (b).



**Figure 7.** 2D (a) and 3D (b) plasmonic crystals of variable width.



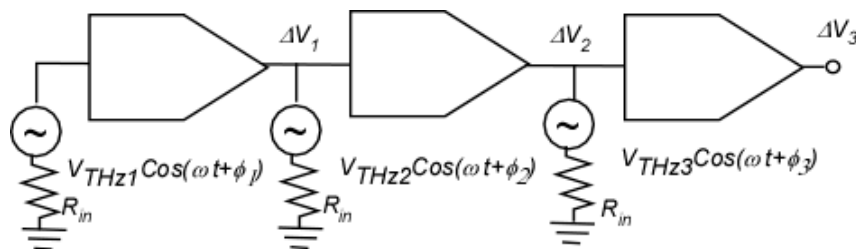
**Figure 8.** Stubs for tuning: (a) ungated stub; (b) stub with a single tuning gate; (c) stub with a split tuning gate; (d) stub with side gates; (e) stub with side gates and top gate; (f) stub with side gate and two top tuning gates.

Figure 6 shows two possible implementations of the plasmonic boom structures. The plasmonic boom instability [19,20] occurs when the electron velocity exceeds the plasma velocity. It is similar to the sonic boom occurring when a jet achieves a supersonic velocity. In a plasmonic crystal, such instability should be very effective if the electron drift velocity repeatedly goes higher and lower than the plasma velocity. In the structure shown in Figure 6a, the plasma frequency is modulated via having the periodic pattern of varying electron densities. In contrast, the structure shown in Figure 6b corresponds to the same plasma frequency spectrum in all the regions. However, the electron drift velocity is higher in narrower regions and smaller in the wider regions. Using narrow protruding regions called plasmonic stubs allows for the phase control in plasmonic 1D, 2D, and 3D plasmonic crystals, schematically shown in Figure 7. The stubs could be gated as shown in Figure 6 and, therefore, tunable, allowing for the optimized phase relations [113].

The tunable transmission by the gated gate structure was described in [114]. The transmission minima at the fundamental plasma frequency and its harmonics were ob-

served in the temperature range from 4.2 K to 170 K. THz generation by a grating gate structure, due to a plasmonic boom instability was proposed, for the first time, in [19] and observed in [115].

The idea of adjusting the phase shifts in the unit cells of a plasmonic crystal for the vector detection of generation could be also applied to a travelling wave amplifier concept [45] (see Figure 9). Feeding the phase-shifted terahertz (THz) signal into the stages of a TeraFET amplifier dramatically increases the response (see Figure 10). The number of stages is only limited by the THz beam cross-section. As seen from Figure 10, this “traveling wave amplifier” approach enables orders of magnitude enhancement in the THz detector responsivity.



**Figure 9.** Schematic of the two-stage TeraFET amplifier detector with the THz signals applied to each stage with a phase shift.

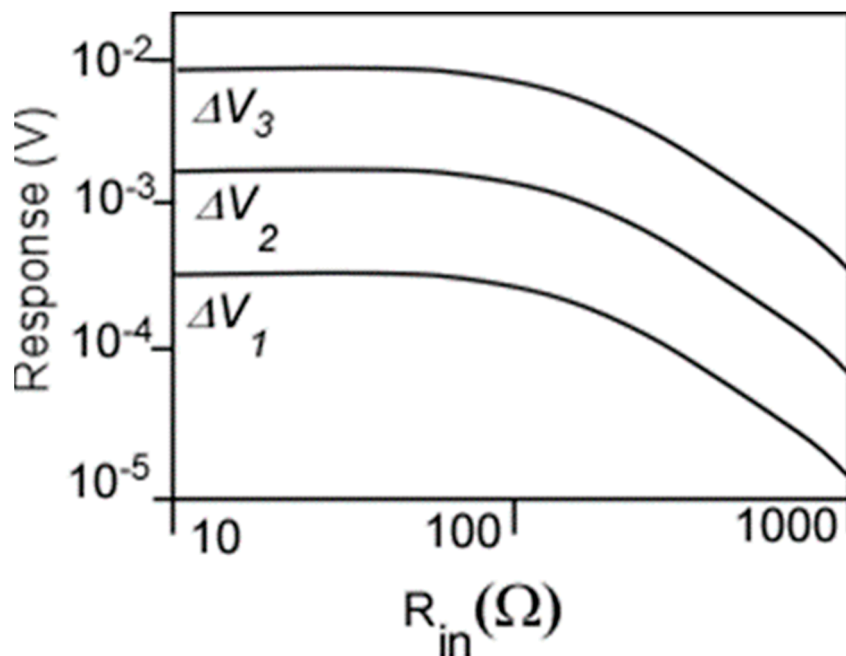


**Figure 10.** Drain response for each stage using harmonic balance (HB) and transient simulation as a function of the THz signal impedance with different schemes and approaches.  $\Delta U_1$ ,  $\Delta U_2$ , and  $\Delta U_3$  are the response at  $V_{d1}$ ,  $V_{d2}$ , and  $V_{d3}$ , respectively (see Figure 9).

#### 4. TeraFET Sources

As mentioned above, the state-of-the-art Si FET emitters using frequency multiplication generate in the order of a hundred of microwatts power in the 300 GHz range [106]. However, the TeraFET output power could be increased using a series connection of TeraFETs [107] and even more by using the plasmonic crystal TeraFETs discussed above with the estimated power output on the order ~100 mW [20]. Table 3 compares the performance of the existing THz electronic sources.

**Table 3.** THz electronic sources operating at 300 K unless stated otherwise (see also [116–127]).

THz Emitter	Frequency (THz)	Output Power (mW) 300 K	DC Power (mW)	Efficiency (%)	Reference
40 nm Si CMOS	0.266	0.69	1790	0.039	[7]
GaAs pHEMT	0.144–0.432	0.063 @300 K 0.278 @77 K	180 (estimated)	0.1	[60]
130 nm SiGe HBTs	0.25	7.08	1960	0.36	[116]
130 nm SiGe BiCMOS	0.34	1.02	1700	0.87	[117]
Schottky diode frequency multipliers	0.05–520	1900–200	-	38–5	[123]
Gunn diodes	0.1–0.3	0.05–0.023	-	-	[124]
IMPATT diodes	0.1–300	400–10	-	-	[125]
Resonant tunnelling diode array	1–1.98	0.7	-	-	[126]
THz plasmon-emitting graphene-channel transistor	1–7.6	0.01 @5.2 THz 0.001 @7.6 THz @100 K	-	-	[127]

Terahertz plasmon amplifying graphene-channel transistors have been also proposed (see [128] and references therein.) Vacuum electronic sources could produce THz radiation in a large range of frequencies and output powers. Free electron lasers generated up to 500 kW peak power [129] in the range of 0.1 to 2.73 THz; BWO lamps generate from 50 mW to 10 kW power in the 0.2 to 0.65 THz range [130]; and klinotrons produce up to watts of power in the range 0.1 to 0.5 THz [131], with gyrotrons producing kilowatts of power in the THz range [132]. However, THz electronic sources, especially Si CMOS, have the highest potential for 6G communications in the 300 GHz band. The progress in developing this technology has been incremental but important. The Si CMOS and BiCMOS plasmonic sources, even in the 300 GHz band, where plasmons quickly decay, have a promise of orders of magnitude improvement by developing circuits with matched phases between the stages (see reference [45] for the description of this concept).

## 5. Other TeraFET Applications

TeraFET technology will also enable THz applications including astronomical science [133–135], earth observation [136], sensing [137–139], chemical analysis [140,141], homeland security, concealed weapon and explosive detection [142,143], industrial controls [144,145], compact radars [146,147], structural integrity testing, spacecraft tiles control [144], Internet of Things (IoT), biotechnology [148–150], medicine [151,152], including cancer diagnostics [153], and non-destructive VLSI testing during the manufacturing process [154] and in-situ checking of the THz scans of chips [155–159]. Artificial intelligence processing of the VLSI THz scans allows distinguishing between genuine and fake VLSI for hardware cyber security applications [158]. Figure 11 shows the THz frequency ranges for different applications of the THz technology.

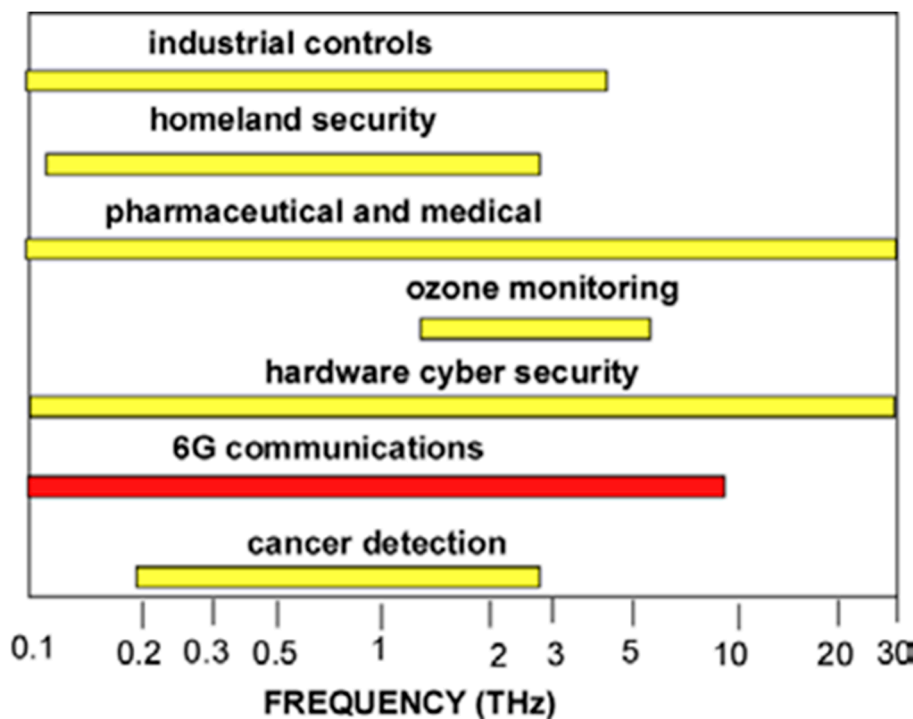


Figure 11. THz frequency ranges for different applications.

The THz range for 6G applications is extended to 10 THz to include communications in space [133] and between computer chips [160]. The development of 6G THz communication technology will be very beneficial for all other THz applications.

## 6. Conclusions

Short-channel TeraFETs and TeraFET plasmonic crystals have great potential for supporting transformational 6G communications technology in the 300 GHz band and beyond. The TeraFET physics involves ballistic or quasi-ballistic transport with the channel dimensions being smaller than or close to the electron mean free path in the TeraFET channel. GaAs plasmonic THz imaging arrays have already been commercialized [161]. Si CMOS deep submicron TeraFETs have also demonstrated excellent performance. This technology could support 300 GHz line-of-sight detectors, travelling wave amplifiers, spectrometers, and generators. III-N-based TeraFETs could find applications in the 6G communication towers because of their potential of delivering a higher power [162,163]. In a longer run, TeraFETs based on novel plasmonic materials, such as graphene, graphene-based heterojunctions, and p-diamond, might compete with GaAs and Si CMOS TeraFETs, and might even extend THz communications to higher THz frequencies.

**Author Contributions:** M.S. contributed to conceptualization and wrote the manuscript; G.A., T.O. and V.R. contributed to conceptualization, methodology, and validation. All authors have read and agreed to the published version of the manuscript.

**Funding:** This work was supported by the U.S. Air Force Office of Scientific Research (No. FA9550-19-1-0355) (Project Manager Dr. Ken Gorecka), Army Research Office (No. W911NF-17-S-0002) (Project Manager Dr. John Qiu), and the Army Research Laboratory under the ARL MSME Alliance (Project Manager Dr. Meredith Reed). The work done by Taiichi Otsuji was supported by the JSPS KAKENHI (Nos. 16H06361, 20K20349, and 21H04546), Japan.

**Institutional Review Board Statement:** Not applicable.

**Informed Consent Statement:** Not applicable.

**Data Availability Statement:** Not applicable.

**Conflicts of Interest:** The authors declare no conflict of interest.

## References

1. Labovitz, C. Early Effects of COVID-19 Lockdowns on Service Provider Networks: The Networks Soldier on! Available online: <https://www.nokia.com/blog/early-effects-covid-19-lockdowns-service-provider-networks-networks-soldier/> (accessed on 20 March 2020).
2. Dhillon, S.S.; Vitiello, M.S.; Linfield, E.H.; Davies, A.; Hoffmann, M.; Booske, J.; Paoloni, C.; Gensch, M.; Weightman, P.; Williams, G.P.; et al. The 2017 terahertz science and technology roadmap. *J. Phys. D Appl. Phys.* **2017**, *50*, 043001. [CrossRef]
3. Chowdhury, M.Z.; Shahjalal, M.; Ahmed, S.; Jang, Y.M. 6G Wireless Communication Systems: Applications, Requirements, Technologies, Challenges, and Research Directions. *IEEE Open J. Commun. Soc.* **2020**, *1*, 957–975. [CrossRef]
4. Zhou, Y.; Liu, L.; Wang, L.; Hui, N.; Cui, X.; Wu, J.; Peng, Y.; Qi, Y.; Xing, C. Service-aware 6G: An intelligent and open network based on the convergence of communication, computing and caching. *Digit. Commun. Netw.* **2020**, *6*, 253–260. [CrossRef]
5. O’Dea, S. Connection Density of 4G, 5G and 6G Technology, 19 November 2020. Available online: <https://www.statista.com/statistics/1183690/mobile-broadband-connection-density/> (accessed on 22 November 2021).
6. Pala, N.; Shur, M. THz Photonic and Plasmonic Devices for Sensing, Imaging and Communication Applications, SPIE Defense + Commercial Sensing. In Proceedings of the Micro- and Nanotechnology Sensors, Systems and Applications XI, Baltimore, MD, USA, 13 May 2019; Volume 10982, p. 109822Y. [CrossRef]
7. Lee, S.; Hara, S.; Yoshida, T.; Amakawa, S.; Dong, R.; Kasamatsu, A.; Sato, J.; Fujishima, M. An 80-Gb/s 300-GHz-Band Single-Chip CMOS Transceiver. *IEEE J. Solid-State Circuits* **2019**, *54*, 3577–3588. [CrossRef]
8. Fujishima, M. Overview of sub-terahertz communication and 300GHz CMOS transceivers. *IEICE Electron. Express* **2021**, *18*, 20212002. [CrossRef]
9. Kürner, T.; Kallfass, I.; Ajito, K.; Kasamatsu, A.; Britz, D.; Priebe, S. “What’s Next? Wireless Communication beyond 60 GHz,” Tutorial of IEEE 802.15 IG THz, IEEE 802 Plenary. 2012. Available online: <https://mentor.ieee.org/802.15/dcn/12/15-12-0320-02-0thz-what-s-next-wireless-communication-beyond-60-ghz-tu-torial-ig-thz.pdf> (accessed on 22 November 2021).
10. Bhat, J.R.; AlQahtani, S.A. 6G Ecosystem: Current Status and Future Perspective. *IEEE Access* **2021**, *26*, 43134–43136. [CrossRef]
11. NTT DOCOMO, Inc. White Paper 5G Evolution and 6G. 2020. Available online: [www.nttdocomo.co.jp/english/binary/pdf/corporate/technology/](http://www.nttdocomo.co.jp/english/binary/pdf/corporate/technology/) (accessed on 22 November 2021).
12. Shur, M. Pandemic Equation for Describing and Predicting COVID-19 Evolution. *J. Health Inform. Res.* **2021**, *5*, 168–180. [CrossRef]
13. IEEE. IEEE Standard for High Data Rate Wireless Multi-Media Networks—Amendment 2:100 Gb/s Wireless Switched Point-to-Point Physical Layer; IEEE Standard 802.15.3d-2017; IEEE: Piscataway, NJ, USA, 2017.
14. Shur, M.; Gaska, R. Device and Method for Managing Radiation. U.S. Patent 7638817, 29 December 2009.
15. Shur, M.; Ryzhii, V.; Gaska, R. Method of Radiation Generation and Manipulation. U.S. Patent 7,619,263, 17 November 2009.
16. Petrov, A.S.; Svintsov, D.; Ryzhii, V.; Shur, M.S. Amplified-reflection plasmon instabilities in grating-gate plasmonic crystals. *Phys. Rev. B* **2017**, *95*, 045405. [CrossRef]
17. Karabiyik, M.; Ahmadivand, A.; Sinha, R.; Al-Amin, C.; Vabbina, P.K.; Kaya, S.; Rupper, G.; Rudin, S.; Shur, M.; Pala, N. Plasmonic properties of asymmetric dual grating gate plasmonic crystals. *Phys. Status Solidi B* **2016**, *253*, 671–675. [CrossRef]
18. Teperik, T.V.; De Abajo, F.J.G.; Popov, V.; Shur, M. Strong terahertz absorption bands in a scaled plasmonic crystal. *Appl. Phys. Lett.* **2007**, *90*, 251910. [CrossRef]
19. Kachorovskii, V.; Shur, M. Current-induced terahertz oscillations in plasmonic crystal. *Appl. Phys. Lett.* **2012**, *100*, 232108. [CrossRef]
20. Aizin, R.; Mikalopas, J.; Shur, M. Current driven “plasmonic” instability in gated periodic ballistic nanostructures. *Phys. Rev. B* **2016**, *93*, 195315. [CrossRef]
21. Dmitriev, A.; Kachorovskii, V.; Shur, M. Granular semiconductor/pyroelectric media as a tunable plasmonic crystal. *Solid-State Electron.* **2007**, *51*, 812–815. [CrossRef]
22. Zhang, X.; Xu, Q.; Xia, L.; Li, Y.; Gu, J.; Tian, Z.; Ouyang, C.; Han, J.; Zhang, W. Terahertz surface plasmonic waves: A review. *Adv. Photonics* **2020**, *2*, 014001. [CrossRef]
23. Karabiyik, M. Terahertz Plasmonic Devices. ProQuest ETD Collection for FIU. AAI10744516. 2017. Available online: <https://digitalcommons.fiu.edu/dissertations/AI10744516> (accessed on 22 November 2021).
24. Aizin, G.; Mikalopas, J.; Shur, M.S. Giant Inverse Faraday Effect in Plasmonic Crystal Ring. *arXiv* **2019**, arXiv:2109.14051. Available online: <http://arxiv.org/abs/2109.14051> (accessed on 20 October 2021).
25. Yeung, K.Y.M.; Chee, J.; Yoon, H.; Song, Y.; Kong, J.; Ham, D. Far-Infrared Graphene Plasmonic Crystals for Plasmonic Band Engineering. *Nano Lett.* **2014**, *14*, 2479–2484. [CrossRef]
26. Daniel, M. Mittleman, Frontiers in Terahertz Sources and Plasmonics Nature Photonics, Volume 7, September 2013. Available online: [www.nature.com/naturephotronics](http://www.nature.com/naturephotronics) (accessed on 22 November 2021).
27. Sugaya, T.; Kawano, Y. Frequency-Tunable Terahertz Plasmonic Structure Based on the Solid Immersed Method for Sensing. *Sensors* **2021**, *21*, 1419. [CrossRef]
28. Zakharko, Y.; Graf, A.; Zaumseil, J. Plasmonic Crystals for Strong Light–Matter Coupling in Carbon Nanotubes. *Nano Lett.* **2016**, *16*, 6504–6510. [CrossRef] [PubMed]

29. Dyer, G.C.; Aizin, G.R.; Preu, S.; Vinh, N.Q.; Allen, S.J.; Reno, J.L.; Shaner, E.A. Inducing an Incipient Terahertz Finite Plasmonic Crystal in Coupled Two Dimensional Plasmonic Cavities. *Phys. Rev. Lett.* **2012**, *109*, 126803. [[CrossRef](#)]
30. Dyer, G.C.; Aizin, G.R.; Allen, S.J.; Grine, A.D.; Bethke, D.; Reno, J.L.; Shaner, E.A. Induced transparency by coupling of Tamm and defect states in tunable terahertz plasmonic crystals. *Nat. Photonics* **2013**, *7*, 925–930. [[CrossRef](#)]
31. Aizin, G.R.; Dyer, G.C. Transmission line theory of collective plasma excitations in periodic two-dimensional electron systems: Finite plasmonic crystals and Tamm states. *Phys. Rev. B* **2012**, *86*, 235316. [[CrossRef](#)]
32. Deng, X.; Li, L.; Enomoto, M.; Kawano, Y. Continuously Frequency-Tunable Plasmonic Structures for Terahertz Bio-sensing and Spectroscopy. *Sci. Rep.* **2019**, *9*, 3498. [[CrossRef](#)] [[PubMed](#)]
33. Schaafsma, M.C.; Rivas, J.G. Semiconductor plasmonic crystals: Active control of THz extinction. In Proceedings of the 2013 38th International Conference on Infrared, Millimeter, and Terahertz Waves (IRMMW-THz), Mainz, Germany, 1 September 2013; pp. 1–2. [[CrossRef](#)]
34. Liu, X.; Ytterdal, T.; Shur, M. Line of sight THz detector using Si TeraFETs. In Proceedings of the 46th IRMMW-THz 2021 Conference, Chengdu, China, 29 August–3 September 2021.
35. Liu, X.; Ytterdal, T.; Shur, M. Travelling Wave THz Spectrometer using Si TeraFETs. In Proceedings of the 46th IRMMW-THz 2021 Conference, Chengdu, China, 29 August–3 September 2021.
36. Rumyantsev, S.; Liu, X.; Kachorovskii, V.; Shur, M. Homodyne phase sensitive terahertz spectrometer. *Appl. Phys. Lett.* **2017**, *111*, 121105. [[CrossRef](#)]
37. Veksler, D.; Muraviov, A.; Stillman, W.; Pala, N.; Shur, M. Detection and Homodyne Mixing of Terahertz Gas Laser Radiation by Submicron GaAs/AlGaAs FETs. In Proceedings of the 2017 IEEE Sensors Conference, Atlanta, GA, USA, 28–31 October 2007; pp. 443–445.
38. Gorbenko, I.; Kachorovski, V.Y.; Shur, M.S. Plasmonic polarization-sensitive detector of terahertz radiation. *J. Phys. Conf. Ser.* **2019**, *1236*, 012029. [[CrossRef](#)]
39. Ikamas, K.; But, D.B.; Lisauskas, A. Homodyne Spectroscopy with Broadband Terahertz Power Detector Based on 90-nm Silicon CMOS Transistor. *Appl. Sci.* **2021**, *11*, 412. [[CrossRef](#)]
40. Gershgorin, B.; Kachorovskii, V.Y.; Lvov, Y.V.; Shur, M.S. Field effect transistor as heterodyne terahertz detector. *Electron. Lett.* **2008**, *44*, 1036–1037. [[CrossRef](#)]
41. Shur, M.S.; Liu, X.; Rumyantsev, S.; Kachorovskii, V. Heterodyne Phase Sensitive Terahertz Spectrometer. In Proceedings of the 2017 IEEE Sensors Conference, Atlanta, GA, USA, 28–31 October 2007; pp. 621–623.
42. Wang, N.; Javadi, H.; Jarrahi, M. Heterodyne terahertz detection with plasmonic photomixers. In Proceedings of the 2016 IEEE MTT-S International Microwave Symposium (IMS), San Francisco, CA, USA, 22–27 May 2016; pp. 1–3. [[CrossRef](#)]
43. Wang, N.; Cakmakyapan, S.; Lin, Y.-J.; Javadi, H.; Jarrahi, M. Room-temperature heterodyne terahertz detection with quantum-level sensitivity. *Nat. Astron.* **2019**, *3*, 977–982. [[CrossRef](#)]
44. Liu, X.; Ytterdal, T.; Shur, M. Frequency to digital conversion using Si TeraFETs. *Opt. Eng.* **2021**, *60*, 082017. [[CrossRef](#)]
45. Liu, X.; Ytterdal, T.; Shur, M. TeraFET amplifier detector. In Proceedings of the 2020 International Topical Meeting on Microwave Photonics (MWP), Matsue, Japan, 24–26 November 2020; pp. 216–219.
46. Tonks, L.; Langmuir, I. Oscillations in Ionized Gases. *Phys. Rev.* **1929**, *33*, 195–210. [[CrossRef](#)]
47. Pines, D.; Bohm, D. A Collective Description of Electron Interactions: II. Collective vs Individual Particle Aspects of the Interactions. *Phys. Rev.* **1952**, *85*, 338–353. [[CrossRef](#)]
48. Stern, A.; Ferrell, R.A. Surface Plasma Oscillations of a Degenerate Electron Gas. *Phys. Rev.* **1960**, *120*, 130. [[CrossRef](#)]
49. Chaplik, A.V. Possible crystallization of charge carriers in low-density inversion layers. *Sov. Phys. JETP* **1972**, *35*, 395.
50. Dyakonov, M.; Shur, M. Shallow water analogy for a ballistic field effect transistor. New mechanism of plasma wave generation by DC current. *Phys. Rev. Lett.* **1993**, *71*, 2465. [[CrossRef](#)] [[PubMed](#)]
51. Dyakonov, M.; Shur, M. Plasma wave electronics: Novel terahertz devices using two dimensional electron fluid. *IEEE Trans. Electron. Devices* **1996**, *43*, 1640–1645. [[CrossRef](#)]
52. Ryzhii, V.; Satou, A.; Shur, M.S. Plasma Instability and Terahertz Generation in HEMTs Due to Electron Transit-Time Effect. *IEICE Trans. Electron.* **2006**, *E89-C*, 1012–1019. [[CrossRef](#)]
53. Knap, W.; Lusakowski, J.; Parenty, T.; Bollaert, S.; Cappy, A.; Popov, V.V.; Shur, M.S. Emission of terahertz radiation by plasma waves in 60 nm AlInAs/InGaAs high electron mobility transistors. *Appl. Phys. Lett.* **2004**, *84*, 2331–2333. [[CrossRef](#)]
54. Lusakowski, J.; Knap, W.; Dyakonova, N.; Varani, L.; Mateos, J.; Gonzalez, T.; Roelens, Y.; Bollaert, S.; Cappy, A.; Karpierz, K. Voltage tunable terahertz emission from a ballistic nanometer InGaAs-InAlAs transistor. *J. Appl. Phys.* **2005**, *97*, 064307. [[CrossRef](#)]
55. Watanabe, T.; Satou, A.; Suemitsu, T.; Knap, W.; Popov, V.V.; Otsuji, T. Plasmonic terahertz monochromatic coherent emission from an asymmetric chirped dual-grating-gate InP-HEMT with photonic vertical cavities. In Proceedings of the CLEO, Conference Lasers Electrooptics Digit, San Jose, CA, USA, 8–13 June 2013; pp. 1–9.
56. Dyakonova, N.E.; El Fatimy, A.; Sakowski, J. Room-temperature terahertz emission from nanometer field-effect transistors. *Appl. Phys. Lett.* **2006**, *88*, 141906. [[CrossRef](#)]
57. Zhou, Y.; Li, X.; Tan, R. Extraction of terahertz emission from a grating-coupled high-electron-mobility transistor. *J. Semicond.* **2013**, *34*, 022002. [[CrossRef](#)]
58. Meziani, Y.M.; Handa, H.; Knap, W.; Otsuji, T.; Sano, E.; Popov, V.; Tsymbalov, G.M.; Coquillat, D.; Teppe, F. Room temperature terahertz emission from grating coupled two-dimensional plasmons. *Appl. Phys. Lett.* **2008**, *92*, 201108. [[CrossRef](#)]

59. Onishi, T.; Tanigawa, T.; Takigawa, S. High power terahertz emission from a single gate AlGaN/GaN field effect transistor with periodic ohmic contacts for plasmon coupling. *Appl. Phys. Lett.* **2010**, *97*, 092117. [\[CrossRef\]](#)
60. Kim, S.; Hong, S.; Jang, J. Strong and narrowband terahertz radiation from GaAs based pHEMT and terahertz imaging. *Microw. Opt. Technol. Lett.* **2020**, *62*, 3791–3795. [\[CrossRef\]](#)
61. Boubanga-Tombet, S.; Teppe, F.; Coquillat, D.; Nadar, S.; Dyakonova, N.; Videlier, H.; Knap, W.; Shchepetov, A.; Gardès, C.; Roelens, Y.; et al. Current driven resonant plasma wave detection of terahertz radiation: Toward the Dyakonov–Shur instability. *Appl. Phys. Lett.* **2008**, *92*, 212101. [\[CrossRef\]](#)
62. Bandurin, D.A.; Svintsov, D.; Gayduchenko, I.; Shuigang, G.; Xu, G.; Principi, A.; Moskotin, M.; Tretyakov, I.; Yagodkin, D.; Zhukov, S.; et al. Resonant terahertz detection using graphene plasmons. *Nat. Commun.* **2018**, *9*, 5392. [\[CrossRef\]](#)
63. Shur, M. Plasmonic heterodimensional resonance for subwavelength imaging. In Proceedings of the SPIE 10639, Micro- and Nanotechnology Sensors, Systems, and Applications X, Orlando, FL, USA, 8 May 2018; Volume 1063907. [\[CrossRef\]](#)
64. Kim, J.; Son, H.; Cho, D.J.; Geng, B.; Regan, W.; Shi, S.; Kim, K.; Zettl, A.; Shen, Y.-R.; Wang, F. Electrical Control of Optical Plasmon Resonance with Graphene. *Nano Lett.* **2012**, *12*, 5598–5602. [\[CrossRef\]](#)
65. Li, Y.; Yan, H.; Farmer, D.B.; Meng, X.; Zhu, W.; Osgood, R.M.; Heinz, T.F.; Avouris, P. Graphene Plasmon Enhanced Vibrational Sensing of Surface-Adsorbed Layers. *Nano Lett.* **2014**, *14*, 1573–1577. [\[CrossRef\]](#)
66. Knap, W.; Deng, Y.; Rumyantsev, S.; Lü, J.-Q.; Shur, M.; Saylor, C.A.; Brunel, L.C. Resonant detection of subterahertz radiation by plasma waves in a submicron field-effect transistor. *Appl. Phys. Lett.* **2002**, *80*, 3433–3435. [\[CrossRef\]](#)
67. Peralta, X.G.; Allen, S.J.; Wanke, M.C.; Harff, N.E.; Simmons, J.A.; Lilly, M.P.; Reno, J.L.; Burke, P.J.; Eisenstein, J.P. Terahertz photoconductivity and plasmon modes in double-quantum-well field-effect transistors. *Appl. Phys. Lett.* **2002**, *81*, 1627. [\[CrossRef\]](#)
68. Knap, W.; Kachorovskii, V.; Deng, Y.; Rumyantsev, S.; Lü, J.-Q.; Gaska, R.; Shur, M.; Simin, G.; Hu, X.; Khan, M.A.; et al. Nonresonant detection of terahertz radiation in field effect transistors. *J. Appl. Phys.* **2002**, *91*, 9346–9353. [\[CrossRef\]](#)
69. Shur, M.S. Plasmonic detectors and sources for THz communication and sensing. *Micro- Nanotechnol. Sens. Syst. Appl. X* **2018**, *10639*, 1063929.
70. Stillman, W.; Donais, C.; Rumyantsev, S.; Shur, M.; Veksler, D.; Hobbs, C.; Smith, C.; Bersuker, G.; Taylor, W.; Jammy, R. Silicon FIN FETs as detectors of terahertz and sub-terahertz radiation. *Int. J. High Speed Electron. Syst.* **2011**, *20*, 27–42. [\[CrossRef\]](#)
71. Lisauskas, A.; Bauer, M.; Boppel, S.; Mundt, M.; Khamaisi, B.; Socher, E.; Venckevičius, R.; Minkevičius, L.; Kašalynas, I.; Seljuta, D.; et al. Exploration of Terahertz Imaging with Silicon MOSFETs. *J. Infrared Millim. Terahertz Waves* **2014**, *35*, 63–80. [\[CrossRef\]](#)
72. Kenneth, K.O.; Chang, M.-C.F.; Shur, M.; Knap, W. Sub-millimeter wave signal generation and detection in CMOS. In Proceedings of the 2009 IEEE MTT-S International Microwave Symposium Digest, Boston, MA, USA, 7–12 June 2009; pp. 185–188.
73. Oje fors, E.; Pfeiffer, U.; Lisauskas, A.; Roskos, H. A 0.65 THz Focal-Plane Array in a Quarter-Micron CMOS Process Technology. *IEEE J. Solid-State Circuits* **2009**, *44*, 1968–1976. [\[CrossRef\]](#)
74. Stillman, W.; Guarin, F.; Kachorovskii, V.Y.; Pala, N.; Rumyantsev, S.; Shur, M.; Veksler, D. Nanometer scale complementary silicon MOSFETs as detectors of terahertz and sub-terahertz radiation. In Proceedings of the 2017 IEEE Sensors Conference, Atlanta, GA, USA, 28–31 October 2007; pp. 479–480.
75. Stillman, W.; Veksler, D.; Elkhatib, T.; Salama, K.; Guarin, F.; Shur, M. Sub-terahertz testing of silicon MOSFET. *Electron. Lett.* **2008**, *44*, 1325–1327. [\[CrossRef\]](#)
76. But, D.; Diakonova, N.; Drexler, C.; Drachenko, O.; Romanov, K.; Golenkov, O.G.; Sizov, F.F.; Gutin, A.; Shur, M.; Ganichev, S.D.; et al. The dynamic range of THz broadband FET detectors. In Proceedings of the SPIE 8846, Terahertz Emitters, Receivers, and Applications IV, San Francisco, CA, USA, 24 September 2013; Volume 884612. [\[CrossRef\]](#)
77. Popov, V.; Ermolaev, D.M.; Maremyanin, K.V.; Maleev, N.A.; Zemlyakov, V.E.; Gavrilenko, V.I.; Shapoval, S.Y. High-responsivity terahertz detection by on-chip InGaAs/GaAs field-effect-transistor array. *Appl. Phys. Lett.* **2011**, *98*, 153504. [\[CrossRef\]](#)
78. Popov, V.; Yermolaev, D.M.; Maremyanin, K.V.; Zemlyakov, V.E.; Maleev, N.A.; Gavrilenko, V.I.; Bespalov, V.A.; Yegorkin, V.I.; Ustinov, V.M.; Shapoval, S.Y. Detection of terahertz radiation by tightly concatenated InGaAs field-effect transistors integrated on a single chip. *Appl. Phys. Lett.* **2014**, *104*, 163508. [\[CrossRef\]](#)
79. Zhang, Y.; Shur, M.S. p-Diamond, Si, GaN, and InGaAs TeraFETs. *IEEE Trans. Electron. Devices* **2020**, *67*, 4858–4865. [\[CrossRef\]](#)
80. Gavrilenko, V.I.; Demidov, E.V.; Marem’yanin, K.V.; Morozov, S.V.; Knap, W.; Lusakowski, J. Electron transport and detection of terahertz radiation in a GaN/AlGaN submicrometer field-effect transistor. *Semiconductors* **2007**, *41*, 232–234. [\[CrossRef\]](#)
81. El Fatimy, A.; Tombet, S.B.; Teppe, F.; Knap, W.; Veksler, D.; Rumyantsev, S.; Shur, M.; Pala, N.; Gaska, R.; Fareed, Q.; et al. Terahertz detection by GaN/AlGaN transistors. *Electron. Lett.* **2006**, *42*, 1342–1344. [\[CrossRef\]](#)
82. Bauer, M.; Ramer, A.; Chevtchenko, S.A.; Osipov, K.Y.; Cibiraite, D.; Pralgauskaitė, S.; Ikamas, K.; Lisauskas, A.; Heinrich, W.; Krozer, V.; et al. A High-Sensitivity AlGaN/GaN HEMT Terahertz Detector with Integrated Broadband Bow-Tie Antenna. *IEEE Trans. Terahertz Sci. Technol.* **2019**, *9*, 430–444. [\[CrossRef\]](#)
83. Shaner, E.A.; Lee, M.; Wanke, M.C.; Grine, A.D.; Reno, J.L.; Allen, S.J. Single-quantum-well grating-gated terahertz plasmon detectors. *Appl. Phys. Lett.* **2005**, *87*, 193507. [\[CrossRef\]](#)
84. Dyer, G.C.; Vinh, N.Q.; Allen, S.J.; Aizin, G.R.; Mikalopas, J.; Reno, J.L.; Shaner, E.A. A terahertz plasmon cavity detector. *Appl. Phys. Lett.* **2010**, *97*, 193507. [\[CrossRef\]](#)
85. Mitin, V.; Ryzhii, V.; Otsuji, T. *Graphene-Based Terahertz Electronics and Plasmonics: Detector and Emitter Concepts*; CRC Press: Boca Raton, FL, USA, 2020.
86. De Abajo, F.J.G. Graphene Plasmonics: Challenges and Opportunities. *ACS Photonics* **2014**, *1*, 135–152. [\[CrossRef\]](#)

87. Grigorenko, A.N.; Polini, M.; Novoselov, K.S. Graphene plasmonics. *Nat. Photonics* **2012**, *6*, 749–758. [[CrossRef](#)]
88. Koppens, F.H.L.; Chang, D.E.; de Abajo, F.J.G. Graphene Plasmonics: A Platform for Strong Light–Matter Interactions. *Nano Lett.* **2011**, *11*, 3370–3377. [[CrossRef](#)] [[PubMed](#)]
89. Ju, L.; Geng, B.; Horng, J.; Girit, C.; Martin, M.; Hao, Z.; Bechtel, H.A.; Liang, X.; Zettl, A.; Shen, Y.R.; et al. Graphene plasmonics for tunable terahertz metamaterials. *Nat. Nanotechnol.* **2011**, *6*, 630–634. [[CrossRef](#)]
90. Boubanga-Tombet, S.; Knap, W.; Yadav, D.; Satou, A.; But, D.B.; Popov, V.V.; Gorbenko, I.V.; Kachorovskii, V.; Otsuji, T. Room-Temperature Amplification of Terahertz Radiation by Grating-Gate Graphene Structures. *Phys. Rev. X* **2020**, *10*, 031004. [[CrossRef](#)]
91. Losurdo, M.; Moreno, F.; Cobet, C.; Modreanu, M.; Pernice, W. Plasmonics: Enabling functionalities with novel materials. *J. Appl. Phys.* **2021**, *129*, 220401. [[CrossRef](#)]
92. Aizin, G.R.; Mikalopas, J.; Shur, M. Plasmonic instabilities in two-dimensional electron channels of variable width. *Phys. Rev. B* **2020**, *101*, 245404. [[CrossRef](#)]
93. Shur, M.; Mikalopas, J.; Aizin, G.R. Compact Design Models of Cryo and Room Temperature Si MOS, GaN, InGaAs, and p-diamond HEMT TeraFETs. In Proceedings of the 2020 IEEE Radio and Wireless Symposium (RWS), San Antonio, TX, USA, 26–29 January 2020; pp. 209–212.
94. Park, D.J.; Zhang, C.; Ku, J.C.; Zhou, Y.; Schatz, G.C.; Mirkin, C.A. Plasmonic photonic crystals realized through DNA-programmable assembly. *Proc. Natl. Acad. Sci. USA* **2015**, *112*, 977–981. [[CrossRef](#)]
95. Liu, X.; Dovidenco, K.; Park, J.; Ytterdal, T.; Shur, M.S. Compact Terahertz SPICE Model: Effects of Drude Inductance and Leakage. *IEEE Trans. Electron. Devices* **2018**, *65*, 5350–5356. [[CrossRef](#)]
96. Vartanian, V.; Zollner, S.; Thean, A.V.-Y.; White, T.; Nguyen, B.-Y.; Prabhu, L.; Eades, D.; Parsons, S.; Desjardins, H.; Kim, K.; et al. Metrology Challenges for 45-nm Strained-Si Device Technology. *IEEE Trans. Semicond. Manuf.* **2006**, *19*, 381–390. [[CrossRef](#)]
97. Venugopal, R.; Goasguen, S.; Datta, S.; Lundstrom, M.S. Quantum mechanical analysis of channel access geometry and series resistance in nanoscale transistors. *J. Appl. Phys.* **2004**, *95*, 292–305. [[CrossRef](#)]
98. Shchepetov, A.; Gardes, C.; Roelens, Y.; Cappy, A.; Bollaert, S.; Boubanga-Tombet, S.; Teppe, F.; Coquillat, D.; Nadar, S.; Dyakonova, N.; et al. Oblique modes effect on terahertz plasma wave resonant detection in InGaAs/InAlAs multichannel transistors. *Appl. Phys. Lett.* **2008**, *92*, 242105. [[CrossRef](#)]
99. Rupper, G.; Rudin, S.; Crowne, F.J. Effects of oblique wave propagation on the nonlinear plasma resonance in the two-dimensional channel of the Dyakonov-Shur detector. In Proceedings of the 2011 International Semiconductor Device Research Symposium (ISDRS), College Park, MD, USA, 7–9 December 2011; pp. 1–2. [[CrossRef](#)]
100. Hosotani, T.; Watanabe, T.; Satou, A.; Otsuji, T. Terahertz Emission from an Asymmetric Dual-Grating-Gate InGaAs High-Electron-Mobility Transistor Stimulated by Plasmonic Boom. In Proceedings of the 2019 44th International Conference on Infrared, Millimeter, and Terahertz Waves (IRMMW-THz), Paris, France, 1–6 September 2019.
101. Otsuji, T.; Shur, M. Terahertz Plasmonics: Good Results and Great Expectations. *IEEE Microw. Mag.* **2014**, *15*, 43–50. [[CrossRef](#)]
102. Clochiatti, S.; Mutlu, E.; Preuss, C.; Kress, R.; Prost, W.; Weimann, N. Broadband THz Detection Using InP Triple-Barrier Resonant Tunneling Diode With Integrated Antenna. In *2021 Fourth International Workshop on Mobile Terahertz Systems (IWMTS)*; IEEE: Piscataway, NJ, USA, 2021; pp. 1–5. [[CrossRef](#)]
103. Takida, Y.; Suzuki, S.; Asada, M.; Minamide, H. Sensitive Continuous-Wave Terahertz Detection by Resonant-Tunneling-Diode Oscillators. In Proceedings of the 2020 45th International Conference on Infrared, Millimeter, and Terahertz Waves (IRMMW-THz), Buffalo, NY, USA, 8–13 November 2020; pp. 1–2. [[CrossRef](#)]
104. Shur, M.; Rudin, S.; Rupper, G.; Dagefu, F.; Brodsky, M. TeraFETs for Terahertz Communications. *Photonics Newslett.* **2019**, *33*, 4–7.
105. Ikamas, K.; But, D.B.; Cesiul, A.; Kołaciński, C.; Lisauskas, T.; Knap, W.; Lisauskas, A. All-Electronic Emitter-Detector Pairs for 250 GHz in Silicon. *Sensors* **2021**, *21*, 5795. [[CrossRef](#)]
106. Vu, T.A.; Fujishima, M. A 300 GHz CMOS Transmitter Front-End for Ultrahigh-Speed Wireless Communications. *Int. J. Electr. Comput. Eng.* **2017**, *7*, 2278–2286. [[CrossRef](#)]
107. Elkhatib, T.A.; Kachorovskii, V.; Stillman, W.J.; Veksler, D.B.; Salama, K.N.; Zhang, X.-C.; Shur, M. Enhanced Plasma Wave Detection of Terahertz Radiation Using Multiple High Electron-Mobility Transistors Connected in Series. *IEEE Trans. Microw. Theory Tech.* **2010**, *58*, 331–339. [[CrossRef](#)]
108. Shur, M.S. *Introduction to Electronic Devices*; John Wiley and Sons: New York, NY, USA, 1996.
109. Assaderaghi, F.; Kop, P.; Hu, C. Observation of velocity overshoot in silicon inversion layers. *IEEE Electron. Device Lett.* **1993**, *14*, 484–486. [[CrossRef](#)]
110. Shur, M.; Rupper, G.; Rudin, S. Ultimate limits for highest modulation frequency and shortest response time of field effect transistor. In Proceedings of the SPIE 10194, Micro- and Nanotechnology Sensors, Systems and Applications IX, Orlando, FL, USA, 18 May 2017; Volume 10194M. [[CrossRef](#)]
111. Lu, J.-Q.; Shur, M.; Hesler, J.; Sun, L.; Weikle, R. A Resonant Terahertz Detector Utilizing a High Electron Mobility Transistor. In Proceedings of the IEDM Technical Digest, San Francisco, CA, USA, 6–9 December 1998; pp. 453–456.
112. Nafari, M.; Aizin, G.R.; Jornet, J.M. Plasmonic HEMT Terahertz Transmitter based on the Dyakonov-Shur Instability: Performance Analysis and Impact of Nonideal Boundaries. *Phys. Rev. Appl.* **2018**, *10*, 064025. [[CrossRef](#)]
113. Aizin, G.R.; Mikalopas, J.; Shur, M.S. Plasmons in Ballistic Nanostructures with Stubs: Transmission Line Approach. *IEEE Trans. Electron. Devices* **2018**, *66*, 126–131. [[CrossRef](#)]

114. Muravjov, A.V.; Veksler, D.B.; Popov, V.V.; Polischuk, O.; Hu, X.; Gaska, R.; Pala, N.; Saxena, H.; Peale, R.E.; Shur, M.S. Temperature dependence of plasmonic terahertz absorption in grating-gate GaN HEMT structures. *Appl. Phys. Lett.* **2010**, *96*, 042105. [[CrossRef](#)]
115. Otsuji, A.; Dubinov, V.; Ya Aleshkin, D.; Svintsov, M.; Ryzhii, S.; Boubanga Tombet, D.; Yadav, A.; Satou, V.; Mitin, M.S.; Shur, V.; et al. Graphene-based van der Waals heterostructures for emission and detection of terahertz radiation. In Proceedings of the SPIE 9856, Terahertz Physics, Devices, and Systems X: Advanced Applications in Industry and Defense, Baltimore, MD, USA, 29 April 2016; p. 985603. [[CrossRef](#)]
116. Rodriguez-Vázquez, P.; Grzyb, J.; Sarmah, N.; Heinemann, B.; Pfeiffer, U.R. A 65 Gbps QPSK one meter wireless link operating at a 225–255 GHz tunable carrier in a SiGe HBT technology. In Proceedings of the IEEE Radio Wireless Symposium, Anaheim, CA, USA, 15–18 January 2018; pp. 146–149.
117. Al-Eryani; Knapp, H.; Kammerer, J.; Aufinger, K.; Li, H.; Maurer, L. Fully integrated single-chip 305–375-GHz transceiver with on-chip antennas in SiGe BiCMOS. *IEEE Trans. Terahertz Sci. Technol.* **2018**, *8*, 329–339. [[CrossRef](#)]
118. Lisauskas, A.; Rämer, A.; Burakevič, M.; Chevtchenko, S.A.; Krozer, V.; Heinrich, W.; Roskos, H.G. Terahertz emission from biased AlGaN/GaN high-electron-mobility transistors. *J. Appl. Phys.* **2019**, *125*, 151614. [[CrossRef](#)]
119. Wang, Z.; Chiang, P.-Y.; Nazari, P.; Wang, C.-C.; Chen, Z.; Heydari, P. A CMOS 210-GHz Fundamental Transceiver with OOK Modulation. *IEEE J. Solid-State Circuits* **2014**, *49*, 564–580. [[CrossRef](#)]
120. Wang, C.; Lu, B.; Lin, C.; Chen, Q.; Miao, L.; Deng, X.; Zhang, J. 0.34-THz Wireless Link Based on High-Order Modulation for Future Wireless Local Area Network Applications. *IEEE Trans. Terahertz Sci. Technol.* **2014**, *4*, 75–85. [[CrossRef](#)]
121. Sengupta, K.; Hajimiri, A. Distributed active radiation for THz signal generation. In Proceedings of the 2011 IEEE International Solid-State Circuits Conference, San Francisco, CA, USA, 20–24 February 2011; pp. 288–289.
122. Sengupta, K.; Hajimiri, A. A 0.28 THz 4 × 4 power generation and beam-steering array. In Proceedings of the 2012 IEEE International Solid-State Circuits Conference, San Francisco, CA, USA, 19–23 February 2012; pp. 256–258.
123. Available online: <https://vadiodes.com/en/frequency-multipliers> (accessed on 19 October 2021).
124. Khalid, A.; Dunn, G.M.; MacPherson, R.F.; Thoms, S.; MacIntyre, D.; Li, C.; Steer, M.J.; Papageorgiou, V.; Thayne, I.G.; Kuball, M.; et al. Terahertz oscillations in an In<sub>0.53</sub>Ga<sub>0.47</sub>As submicron planar Gunn diode. *J. Appl. Phys.* **2014**, *115*, 114502. [[CrossRef](#)]
125. Available online: <https://terasense.com/products/> (accessed on 19 October 2021).
126. Asada, M.; Suzuki, S. Terahertz Emitter Using Resonant-Tunneling Diode and Applications. *Sensors* **2021**, *21*, 1384. [[CrossRef](#)]
127. Yadav, D.; Tamamushi, G.; Watanabe, T.; Mitsushio, J.; Tobah, Y.; Sugawara, K.; Dubinov, A.A.; Satou, A.; Ryzhii, M.; Ryzhii, V.; et al. Terahertz light-emitting graphene-channel transistor toward single-mode lasing. *Nanophotonics* **2018**, *7*, 741–752. [[CrossRef](#)]
128. Boubanga-Tombet, S.A.; Satou, A.; Yadav, D.; But, D.B.; Knap, W.; Popov, V.V.; Gorbenko, I.V.; Kachorovskii, V.; Otsuji, T. Paving the Way for Tunable Graphene Plasmonic THz Amplifiers. *Front. Phys.* **2021**, *9*, 726806. [[CrossRef](#)]
129. Gavrilov, N.G.; Knyazev, B.A.; Kolobanov, E.I. Status of the Novosibirsk high-power terahertz FEL. *Nucl. Instrum. Methods Phys. Res.* **2007**, *575*, 54–57. [[CrossRef](#)]
130. He, W.; Zhang, D.L.; Bowes, H.; Yin, K.; Ronald, A.D.; Phelps, R.; Cross, A.W. Generation of broadband terahertz radiation using a backward wave oscillator and pseudospark-sourced electron beam. *Appl. Phys. Lett.* **2015**, *107*, 133501. [[CrossRef](#)]
131. Development of MW & THz Klinotrons. Available online: <http://ire.kharkov.ua/Mysite/HTML/p0019.htm> (accessed on 19 October 2021).
132. Thumm, M. State-of-the-Art of High-Power Gyro-Devices and Free Electron Masers. *J. Infrared Millim. Terahertz Waves* **2020**, *41*, 1–140. [[CrossRef](#)]
133. de Maagt, P.; Bolivar, P.H.; Mann, C. Terahertz Science, Engineering and Systems—From Space to Earth Applications. *Encycl. RF Microw. Eng.* **2005**. [[CrossRef](#)]
134. Siegel, P.H. THz for space: The golden age. In Proceedings of the 2010 IEEE MTT-S International Microwave Symposium, Anaheim, CA, USA, 27 January 2010; pp. 816–819. [[CrossRef](#)]
135. Xia, B.G.; Zhang, D.H.; Meng, J.; Huang, J.; Yao, C.F.; Zhang, J.S. Terahertz FSS for space borne passive remote sensing application. *Electron. Lett.* **2013**, *49*, 1398–1399. [[CrossRef](#)]
136. Waters, J. Submillimeter-wavelength heterodyne spectroscopy and remote sensing of the upper atmosphere. *Proc. IEEE* **1992**, *80*, 1679–1701. [[CrossRef](#)]
137. Shur, M.S. Terahertz Plasmonic Technology. *IEEE Sens. J.* **2021**, *21*, 12752–12763. [[CrossRef](#)]
138. Akter, N.; Pala, N.; Knap, W.; Shur, M. Chapter 8: THz Plasma Field Effect Transistor Detectors, in *Fundamentals of Terahertz Devices and Applications*; Pavlidis, D., Ed.; Wiley: Hoboken, NJ, USA, 2021.
139. Matsura, Y.; Suzuki, T.; Katagiri, T. Terahertz gas sensing based on time-domain-spectroscopy using a hollow-optical fiber gas cell. *Opt. Fibers Sens. Med. Diagn. Treat. Appl. XVIII* **2018**, *10488*, 1048808. [[CrossRef](#)]
140. Kiwa, T.; Kamiya, T.; Morimoto, T.; Fujiwara, K.; Maeno, Y.; Akiwa, Y.; Iida, M.; Kuroda, T.; Sakai, K.; Nose, H.; et al. Imaging of Chemical Reactions Using a Terahertz Chemical Microscope. *Photonics* **2019**, *6*, 10. [[CrossRef](#)]
141. Yang, L.; Guo, T.; Zhang, X.; Cao, S.; Ding, X. Toxic chemical compound detection by terahertz spectroscopy: A review. *Rev. Anal. Chem.* **2018**, *37*, 410. [[CrossRef](#)]
142. Chen, Y.; Liu, H.; Fitch, M.J.; Osiander, R.; Spicer, J.B.; Shur, M.; Zhang, X.C. *THz Diffuse Reflectance Spectra of Selected Explosives and Related Compounds, Passive Millimeter-Wave Imaging Technology VIII*; Roger, A., David, A.W., Eds.; International Society for Optics and Photonics: Bellingham, WA, USA, 2005; Volume 5790, pp. 19–24.

143. Federici, F.; Schulkin, B.; Huang, F.; Gary, D.; Barat, R.; Oliveira, F.; Zimdars, D. THz imaging and sensing for security applications-explosives, weapons, and drugs. *Semicond. Sci. Technol.* **2005**, *20*, S266. [[CrossRef](#)]
144. Zhong, H.; Karpowicz, N.; Xu, J.; Deng, Y.; Ussery, W.; Shur, M.; Zhang, X.-C. Inspection of space shuttle insulation foam defects using a 0.2 THz Gunn diode oscillator, Infrared and Millimeter Waves. In Proceedings of the 12th International Conference on Terahertz Electronics, Karlsruhe, Germany, 27 September 2004; pp. 753–754.
145. Lee, E.S.; Moon, K.; Lee, I.M.; Park, D.W.; Choi, D.H.; Shin, J.H.; Kim, H.S.; Choi, D.H.; Park, K.H. Terahertz Non-destructive Testing Technology for Industrial Applications. *Electron. Telecommun. Trends* **2018**, *33*, 59–69.
146. Ruengwaree, A.; Ghose, A.; Weide, J.; Kampa, G. Ultra-fast pulse transmitter for UWB microwave radar. In Proceedings of the European Radar Conference, Manchester, UK, 13–15 September 2006; IEEE: Piscataway, NJ, USA; pp. 354–357.
147. Nguyen, C.; Han, J. *Time-Domain Ultra-Wideband Radar, Sensor and Components: Theory, Analysis and Design*; Springer Science & Business Media: Berlin/Heidelberg, Germany, 2014.
148. Sun, Q.; He, Y.; Liu, K.; Fan, S.; Parrott, E.P.J.; Pickwell-MacPherson, E. Recent advances in terahertz technology for biomedical applications. *Quant. Imaging Med. Surg.* **2017**, *7*, 345–355. [[CrossRef](#)] [[PubMed](#)]
149. Heilweil, E.; Plusquellec, D. *Terahertz Spectroscopy of Biomolecules*; CRC Press: Boca Raton, FL, USA, 2007; pp. 269–297.
150. Shur, M.S. Subterahertz and terahertz sensing of biological objects and chemical agents. *Terahertz RF Millim. Submillim.-Wave Technol. Appl. XI* **2018**, *10531*, 1053108. [[CrossRef](#)]
151. Siegel, P.H. Terahertz Technology in Biology and Medicine. *IEEE Trans. Microw. Theory Tech.* **2004**, *52*, 2438–2447. [[CrossRef](#)]
152. Hintzsche, H.; Jastrow, C.; Kleine-Ostmann, T.; Kärst, U.; Schrader, T.; Stopper, H. Terahertz Electromagnetic Fields (0.106 THz) Do Not Induce Manifest Genomic Damage In Vitro. *PLoS ONE* **2012**, *7*, e46397. [[CrossRef](#)]
153. Yu, C.; Fan, S.; Sun, Y.; Pickwell-MacPherson, E. The potential of terahertz imaging for cancer diagnosis: A review of investigations to date. *Quant. Imaging Med. Surg.* **2012**, *2*, 33–45. [[CrossRef](#)]
154. Farooq, M.; Shur, M. Inspection System and Method for Detecting Defects at a Materials Interface. U.S. Patent 10,215,695 B1, 26 February 2019.
155. Rupper, G.; Suarez, J.; Rudin, S.; Reed, M.; Shur, M. Terahertz Plasmonics for Testing Very Large-Scale Integrated Circuits under Bias. U.S. Patent 10,890,618 B2, 12 January 2021.
156. Shur, M.; Rudin, S.; Rupper, G.; Reed, M.; Suarez, J. Sub-terahertz testing of millimeter wave Monolithic and very large scale integrated circuits. *Solid-State Electron.* **2019**, *155*, 44–48. [[CrossRef](#)]
157. Akter, N.; Karabiyik, M.; Shur, M.; Suarez, J.; Pala, N. AI Powered THz VLSI Testing Technology. In Proceedings of the 2020 IEEE 29th North Atlantic Test Workshop (NATW), Albany, NY, USA, 18–20 May 2020; pp. 1–5. [[CrossRef](#)]
158. Akter, N.; Siddiquee, M.R.; Shur, M.; Pala, N. AI-Powered Terahertz VLSI Testing Technology for Ensuring Hardware Security and Reliability. *IEEE Access* **2021**, *9*, 64499–64509. [[CrossRef](#)]
159. Shur, M.S.; Suarez, J. Nanoscale silicon MOSFET response to THz radiation for testing VLSI. In Proceedings of the 2018 IEEE 27th North Atlantic Test Workshop (NATW), Essex, VT, USA, 7–9 May 2018; pp. 1–6. [[CrossRef](#)]
160. Deng, Y.; Shur, M.S. Electron mobility and terahertz detection using silicon MOSFETs. *Solid-State Electron.* **2003**, *47*, 1559–1563. [[CrossRef](#)]
161. Available online: <https://terasense.com/products/sub-thz-imaging-cameras/> (accessed on 11 November 2011).
162. Shur, M. AlGaN/GaN plasmonic terahertz electronic devices. *J. Phys.* **2014**, *486*, 012025. [[CrossRef](#)]
163. Ahi, K. Review of GaN-based devices for terahertz operation. *Opt. Eng.* **2017**, *59*, 090901. [[CrossRef](#)]